IDENTIFICATION OF STRUCTURAL STIFFNESS IN BUMP-TYPE FOIL BEARINGS

Dario Rubio
Research Assistant
Dariorubio10@tamu.edu

Dr. Luis San Andres
Professor
Lsanadres@mengr.tamu.edu

Turbomachinery Laboratory
Texas A&M University
College Station, TX 77843

RESUMEN

Las chumaceras de lámina corrugada (FB) cubren muchas de las exigencias de turbomáquinas operando sin lubricantes líquidos. Sin embargo, el diseño de este tipo de chumaceras es todavía empírico a pesar de su aparente éxito en aplicaciones comerciales. El presente artículo presenta experimentos para identificar la rigidez estructural de este tipo de chumaceras. Los experimentos estáticos son realizados sobre dos chumaceras de lámina, tipo-corrugado, cuya longitud y diámetro interno son 1.50"; la lámina tope, tiene un espesor de 0.004" y es recubierta con teflón, y sostenida por 25 laminas corrugadas como soporte estructural. El huelgo radial nominal entre la chumacera y el rotor es de 1.4 mil para un diámetro de 1.500". Los experimentos consisten en aplicar carga estáticas sobre la chumacera a lo largo de ocho posiciones angulares, separadas 45 °. El desplazamiento resultante es registrado con un sensor de corrientes inducidas. El procedimiento es repetido con distintos tipos de precarga, utilizando diámetros de rotor iguales a 1.500", 1.499" y 1.501".

Los resultados experimentales de carga estática y desplazamiento muestran un comportamiento no lineal cuya pendiente (rigidez estructural) aumenta a medida que la carga estática se incrementa. La rigidez estructural se ve afectada significativamente por la precarga ejercida por los distintos rotores, particularmente con pequeñas cargas estáticas, y por la posición angular a la cual la carga estática es aplicada. Experimentos con aumento y reducción graduales de la fuerza estática revelan histéresis mecánica.

ABSTRACT

Compliant foil gas bearings (FB) satisfy many of the requirements noted for novel oil-free turbomachinery. However, FB design remains largely empirical, in spite of successful commercial applications. This paper presents experiments to identify the structural stiffness of bump-type foil bearings. The test foil bearings, 1.50 in length and diameter, contain a single top foil; Teflon® coated, supported on 25 bumps. The nominal radial clearance is 1.4 mils for a 1.5" journal. Tests consist of applying loads on the bearing along eight angular positions equally spaced (45°), and a displacement transducer recording the ensuing bearing (bumps) deflection. The effects of the assembly bearing preload on the bearing stiffness are also determined by conducting static tests with three different shafts, one of 1.5" diameter; and the other two with +1 mil and –1 mil larger (smaller) diameters.

The load versus deflection data reveals a nonlinear and hardening structural stiffness, with significant variations depending on the assembly preload or initial fit and the magnitude of the applied load. Larger variations result from the orientation of the load relative to the location of the top foil spot weld. Loading and unloading tests also evidence hysteresis. The test FB stiffnesses obtained from two bearings, identical in construction, also differ. The assembly preload results in notable stiffness changes, in particular for small radial loads.

NOMENCLATURE

D_i	Journal diameter [in]
F	Static load [lb]
K	Structural foil bearing stiffness [lb/mil]
K_A	Average structural stiffness [lb/mil]
K_{OA}	Overall structural stiffness average [lb/mil]
N	Number of data set points
SEE	Standard error of an estimate [lb/mil]
U_F	Uncertainty of the dynamometer [lb]
U_k	Bearing stiffness uncertainty [lb/mil]
U_V	Uncertainty of the multimeter [V]
x	Foil bearing deflection [mil]
X,Y	Inertial coordinate system
θ	Foil bearing angular position angle [degree]

INTRODUCTION

Over the past 30 years, gas foil bearing technology has paved the way to novel oil-free turbomachinery applications. More reliable and simpler bearing systems able to sustain higher rotational speeds and load capacities are highly desirable. Extreme operating temperatures also limit the use of liquid lubricant bearings. Conversely, gas film bearings have demonstrated sustained efficient operation in high speed turbomachinery applications [1], cryogenic turbo expanders [2, 3] and high-temperature environments [4]; increasing tenfold machinery reliability in comparison to rolling elements bearings.

Bump-type foil bearings consist of a smooth coated top foil supported by corrugated foil (bump foil) strips. The bump foil strips are welded at one end of the bearing housing and are free at the other end, as depicted in Figure 1. The main components of the test foil bearings are:

a) *Bearing Sleeve:* rigid ring supporting the bump foils and the top foil.

b) *Top foil:* thin flat metal sheet attached to the bearing sleeve at one end and free at the other end.

c) *Bumps:* four strips, each with five bumps, aligned axially. The end of a strip is welded to the bearing sleeve while the other end is free. A total of five segments are placed around the bearing sleeve. Note that each segment is welded at one end and free at the other.

d) *Spot Weld:* weld line attaching the top foil and the bump foil strips to the bearing sleeve. The spot weld location is characterized by the absence of bumps and it spans approximately 10°. The spot weld constrains the movement of the top foil and the bump foil at one end (fixed end).

In general, due to the hydrodynamic film created by rotor spinning, the top foil and elastic structure retract resulting in a larger film thickness than with rigid wall bearings [5, 6]. The compliant foil bearing also allows larger shaft misalignments than with fixed geometry bearings. Note that the bump foils act as springs providing a tunable structural stiffness source [7, 8, 9], and damping of Coulomb type arises due to the relative motion between the bumps and the top foil or between the bumps and the bearing wall [10, 11].

Measurement of the structural compliance in bump-foil bearings is the scope of the present study. Ku and Heshmat [8, 9] provide the earliest experimental and analytical studies. Bump material and its pitch and height, and to a lesser extent bump thickness, largely determine the bump stiffness. Coatings with large friction coefficients, surface finish and tight assemblies also produce high values of bump stiffness. The presence or absence of lubrication does not make a remarkable difference in the bump stiffness. Ku [12] evaluates structural stiffness of bump foil strips for several test conditions, i.e. friction coefficient, surface coating, and lubricant, among others. For all test conditions, the dynamic structural stiffness increased as the static load increases, while becoming smaller as the amplitude of motion increased. Ku et al. [7, 10] introduce a model for estimation of the elastic deformation of a bump - foil strip and prediction of the equivalent structure stiffness and viscous damping coefficient. Iordanoff [9] also advances approximate formulae for evaluation of the bump foil stiffness for free end and clamped end (welded) conditions. Typical analyses of bump strips include the friction forces between the top foil and bumps, the housing and bumps, and the coupling forces with adjacent bumps.

There is no published information on the structural stiffness of an entire foil bearing. This stiffness and resulting bearing load capacity are the maximum available since, in operation, hydrodynamic effects merely act as a load path from the rotor to the bearing support casing. This investigation provides reliable measurements of the static structural stiffness of bump-type foil bearings. The results serve as benchmark for calibration of analytical tools under development.

EXPERIMENTAL PROCEDURE

Two bump-type foil bearings were tested to identify their structural parameters. Figure 1 shows the basic elements of the two test bearings, hereby referred as FB1 and FB2. The bearings, 1.50 inches in length and diameter, contain a single foil (0.004”); Teflon® coated, supported on 25 bumps, each of height and pitch equal to 0.015” and 0.18”, respectively. The nominal radial clearance is 1.4 mils for a 1.5 inches journal.

Static tests were performed in a simple test setup on a lathe; see Figure 2, consisting of the test foil bearing, a copper (non-rotating) shaft, a dynamometer, and an eddy current displacement sensor. The load application mechanism consists of moving the dynamometer horizontally toward the foil bearing sleeve. Once the dynamometer touches the bearing, the loading process starts from 0 lb to 50 lb. Notice that a reasonable time between individual loading processes is taken to ensure truly static displacement measurements. The loading process is performed along eight angular positions 45º apart from each other. Thus, angular positions (P1) through (P8) are defined for description. See Figure 3 for a graphical description of these positions relative to the spot weld in the foil bearing. The reference angular coordinate (θ) is measured from the free end to the fixed end of the top foil.

The effects of the assembly bearing preload on the bearing structural stiffness are also determined by conducting static tests with three different shafts, one of 1.5” diameter (D_1); and the other two with +1 mil and –1 mil larger (smaller) diameters, D_2 and D_3, respectively.

Structural characteristics can be identified from these experiments. Bearing deflection-versus-static load curves are later displayed for FBs 1 and 2. Deflection (x) versus force (F) curves corresponding to applied loads 180° apart are grouped as paired measurements, i.e. positions 1 and 5 are displayed on the same curve, for example.

Load versus deflection polynomials, $F=g(x)$, representing the measurements are obtained from the test data for each angular position and journal diameter. The bearing structural

stiffness is identified from

$$K = \frac{\partial F}{\partial x} \quad (1)$$

i.e., by taking the slope of the load (F) versus deflection (x) curve for each test condition.

EXPERIMENTAL RESULTS AND DISCUSSION

During the tests, the static cross-coupled bearing deflection was negligible compared to the direct deflection. Figures 4 and 5 display the recorded deflections for FB1 for all angular positions, and for journal diameters equal to D_1 and D_2, respectively. Figure 6 shows similar results for FB2, but using journal diameter D_3. Each figure displays the bearing deflection versus applied load for four test positions along meridional planes. The negative and positive values of static load do not indicate compression nor traction forces on the bearing.

Variable stiffnesses result when the applied load changes since the foil bearing construction introduces a piece-wise linear characteristic in the bump deformation process with respect to the applied load;. This non linear characteristic on the foil bearing deflection arises when the bearing starts being squeezed against the rigid shaft. At light static loads, only a few bumps are active (compressed) due to the fact that the static load is not large enough to deform bumps far away from the position of static load application. The area of contact between the bearing and the shaft increases as the static load increases, and thus more bumps become activate. The bumps are positioned as parallel springs supporting the journal, and each time a bump stiffness becomes activate, the overall stiffness increases.

For journal diameters equal to D_1 and D_3, the static load versus bearing deflection curve at position 1 (0º, negative values of position 1-5 curve) is particularly different from the results obtained for other angular positions, as shown in Figures 4 and 6. At P1 (θ = 0º), the load pushes the bearing into the shaft at the spot weld, as depicted in Figure 1. Hence, the top foil and bumps around the spot weld are being compressed. The bumps located at the fixed end are more constrained than the bumps located at the free end. The foil bearing, when subjected to small loads applied at the location of the spot weld, tends to move toward the free end since the bumps near this angular position provide less resilience to the movement than the bumps located at the fixed end [10, 11]. Once the load increases, the bumps in the fixed end become active and the bearing develops larger stiffnesses. Although results at position 1 (0º) show a different pattern, the deflection versus load still follows a non linear behavior. On the contrary, preloading the bearing (using journal diameter D_2) eliminates the peculiar deformation behavior at P1 (0º), as shown in Figure 5. The bearing preload expands the top foil and compresses (retracts) the bumps even before the loading process starts. Therefore, the bumps at the free and fixed end become active simultaneously.

For all test conditions, the deformation structural mechanism for both bearings is clearly non linear. A polynomial curve fit establishes an analytical relation between the static load and the bearing deflection; i.e. $F = g(x)$. This relation is given by a third order polynomial and obtained for all pairs of angular orientations as

$$F = a.x^3 + b.x^2 + c.x + d \quad (2)$$

where a, b , c and d are curve fit coefficients determined from the test data. The structural stiffness is, then, identified using Eq. 1. Table 1 gives the structural stiffness equations for all test conditions. The correlation coefficients of the polynomial approximation, i.e. goodness of the curve fit to the test data, exhibit values larger that 99.3% for all test conditions.

Figures 7 and 8 show the structural stiffness for the three journal diameters; and corresponding to FB1 and FB2, respectively. Load positions 4–8 (135°-315°) are displayed on the figures. Remarkable differences in the foil bearing structural stiffness are distinguished when using the different journal diameters. When the shaft diameter is D_3 (1.499”), the bearing stiffness exhibits the widest curve and presents the lowest structural stiffness values. For the nominal shaft diameter D_1 (1.500”), the bearing stiffness increases relative to the D_3 structural stiffness curve for any magnitude of bearing deflection. The higher structural stiffnesses are identified when the foil bearing is preloaded, i.e. with a journal diameter equal to D2 (1.501”). The effect of the shaft diameter on the structural stiffness follows the same pattern for other angular positions. Table 2 shows the maximum and minimum values of bearing structural stiffness at each angular position for the three journal diameters. Maximum and minimum structural stiffness are identified at maximum and minimum static loads, respectively. Note that the bearing preload results in important changes in the FB stiffness, in particular for small load conditions. Rubio [13] describes the uncertainty analysis determining the accuracy of the structural stiffness values identified.

Figures 9.a and 9.b show the FB1 and FB2 structural stiffness for all angular positions. Structural stiffnesses are shown for two loads (50 lb and 5 lb, large and small) and the three journal diameters. The different journal diameters, inducing increasing assembly preload, render significant differences on the structural stiffnesses throughout the load span. Note that a preload (D_2) produces the highest structural stiffness at light loads, while the lowest stiffnesses are for the smallest shaft, D_3, at any static load. The influence of the initial gap between the journal and the foil bearing (assembly preload) covers the whole load range.

A structural stiffness average (K_A), representative of the foil bearing circumference, is calculated for each journal diameter. The highest structural stiffness average in both bearings is identified when the bearing is preloaded (D_2), i.e. for 50 lb and 5 lb, K_A is 35.55 lb/mil and 11.28 lb/mil,

respectively. A similar finding is noted for all other static loads. An overall stiffness average (K_{OA}) is also obtained from the individual structural stiffness average (K_A) for each journal diameter. The standard error of an estimate (*SEE*) shows the goodness of (K_A) and the overall stiffness average (K_{OA}).). The *SEE*, represents the deviation of the average structural stiffness from the data set, i.e.

$$SEE = \left[\frac{\sum_{i=1}^{N} [K_i - K_A]^2}{N-2} \right]^{1/2} \quad (3)$$

where N is the number of data set points. K_A is the average structural stiffness and K_i represent the value of structural stiffness at each data set point.

The highest *SEE* percentages occur at low loads for both bearings. However, FB2 has a smoother stiffness behavior at light loads along all angular positions than FB1, i.e. the overall *SEE* percentage for FB2 is 7.4 % while for the FB1 is 24 %. At high loads both bearings act similarly with respect to the angular loading positions.

In addition to the bearing structural stiffness, hysteresis is also a relevant mechanical characteristic evidencing dry-friction damping. To identify such behavior the foil bearings are loaded and unloaded in the same set of measurements. Ku et al [8] describe the hysteresis as a result of Coulomb damping inherent to the foil bearing construction. Dry-friction damping is produced by the sliding between the top foil and the bump foils while in contact, and also by the bump foils and the bearing sleeve.

Figure 10 shows the recorded hysteresis when loading and unloading FB1 along positions 1– 5. Friction forces between the foil surfaces restrain the movement of the bump foil and the top foil when the bearing is being unloaded; therefore the unloading path follows a different direction than the loading path. Note that the structural stiffness during the loading process is different than during the unloading process, as also reported in [8].

Finally, Figure 11 shows that the bearing structural stiffness varies linearly with respect to the static load, in particular for large forces. The figure also shows that the bearing preload does not alter greatly the bearing stiffness coefficients for a large static load. Bearing preload does affect greatly the stiffness at small loads, however.

CONCLUSIONS

Gas foil bearings satisfy most requirements noted for oil-free turbomachinery applications. However, there is a noticeable absence of experimental verification for the rotordynamic performance of gas foil bearings, including the bearing underlying elastic structural properties. The open literature provides little insight except for infamous commercial claims.

Two commercial bump foil bearings (FBs) were tested for identification of their structural stiffness. The bearings, with length equal to 1.50", consist of a Teflon® coated foil (0.004" thickness) supported on 25 bumps, whose height and pitch equal 0.015" and 0.18", respectively. The FBs are designed to operate with a shaft of nominal diameter equal to 1.50". The manufacturer provided a radial clearance of 1.4 mils for the nominal configuration. A simple test set up was assembled to measure the FB deflections resulting from increasing static loads applied radially at various angular positions around the bearing. The experiments were conducted with three shafts, one with the nominal diameter of 1.50"; and the other shafts with diameters +1 mil and –1 mil larger (smaller) than the nominal one. The different shafts induce a degree of preload into the FB.

The static measurements show different deflection versus load characteristics depending on the orientation of the applied static load relative to the position of the foil spot weld. The experimental results also demonstrate that the structural deflection is nonlinear relative to the applied load. A third degree polynomial in displacement describes well the recorded behavior. Static loading and unloading tests evidence a characteristic hysteresis due to the dry friction between the bumps and the bearing housing. The foil bearing structural stiffness derived from the load versus deflection tests increases nonlinearly as the radial deflection increases (hardening effect). The identified structural stiffness coefficients obtained from two bearings, identical in construction, also differ. The radial preload results in important changes in the FB stiffness, in particular for small load conditions.

ACKNOWLEDGEMENTS

The authors acknowledge the support of the Turbomachinery Research Consortium (TRC) and National Science Foundation (NSF). Thanks to Foster Miller Technologies for providing the test foil bearings.

REFERENCES

[1] Heshmat, H., 1994, "Advancements in the Performance of Aerodynamic Foil Journal Bearings: High Speed and Load Capability," ASME Journal of Tribology, Vol. 116, pp. 287 – 295.

[2] Gu, A., 1988, "Process Fluid Foil Bearing Liquid Hydrogen Turbopump," AIAA/ASME/SAE/ASEE 24th Joint Propulsion Conference, Boston, Massachusetts, Paper No. 88-3130.

[3] Elrod, D., 1997, "Advanced Analysis of Bending Foil Bearing for Cryogenic Applications," 33rd AIAA/ASME/SAE/ASEE Joint Propulsion Conference, Seattle, WA, Paper No. 97-3100.

[4] DellaCorte, C., J.M., Valco, K.C., Radil, and, H., Heshmat, 1999, "Performance and Durability of High Temperature Foil Air Bearing for Oil-Free Turbomachinery," NASA/TM 209187.

[5] Heshmat, H., J., Walomit, and, O., Pinkis, 1983, "Analysis of Gas-Lubricated Compliant Journal Bearings," Journal of Lubrication Technology, Vol. 105, 4, pp. 647-655.

[6] Peng, J.-P, and, M., Carpino, 1993, "Calculation of Stiffness and Damping Coefficient for Elastically Supported Gas Foil Bearings," Journal of Tribology, Transactions of the ASME, Vol. 115, No. 1, pp. 20-27
[7] Ku, C.-P, and, H., Heshmat, 1992, "Complaint Foil Bearing Structural Stiffness Analysis Part I: Theoretical Model - Including Strip and Variable Bump Foil Geometry," ASME Journal of Tribology, Vol. 114, No. 2, pp. 394-400.
[8] Ku, C.-P, and, H., Heshmat, 1993, "Complaint Foil Bearing Structural Stiffness Analysis Part II: Experimental Investigation," ASME Journal of Tribology, Vol. 113, No. 3, pp. 364-369.
[9] Iordanoff, I., 1999, "Analysis of an Aerodynamic Complaint Foil Thrust Bearing: Method for a Rapid Design," ASME Journal of Tribology, Vol. 121, pp. 816-822.
[10] Ku, C.-P, and, H., Heshmat, 1994, "Structural Stiffness and Coulomb Damping in Compliant Foil Journal Bearing: Theoretical Considerations," STLE Tribology Transactions, Vol. 37, No. 3, pp. 525-533
[11] Ku, C.-P, and, H., Heshmat, 1994, "Structural Stiffness and Coulomb Damping in Compliant Foil Journal Bearing: Parametric Studies," STLE Tribology Transactions, Vol. 37, No. 3, pp. 455-462.
[12] Ku, C-P. R., "An Experimental and Theoretical Study of the Dynamic Structural Stiffness in Compliant Foil Journal Bearings," ASME 14th Biennial Conference on Mechanical Vibration and Noise, Albuquerque, NM, DE-Vol. 63, *Vibration of Mechanical Systems and the History of Mechanical Design*, pp. 83-88, September 1993.
[13] Rubio, D., "Measurement of Static Structural Stiffness of Bump-Type Foil Gas Bearings," Undergraduate Senior Honor Thesis, Texas A&M University, Mechanical Engineering Department, August 2002.

Table 1. FB2 derived equations of structural stiffness versus deflection for the three shaft diameters

Journal Diameter	Angular Positions	K [lb/mil] versus *x* [mil] Equations	*x* Range [mil]
D_1 1.500"	1 – 5	$k = 1.308x^2+1.386x + 2.76$	[-5.00 , 4.10]
	2 – 6	$k = 1.695x^2+0.796x+5.265$	[-4.05 , 4.65]
	3 – 7	$k = 1.581x^2-1.11x+ 2.157$	[-4.15, 4.05]
	4 – 8	$k = 1.713x^2+0.06x+ 2.99$	[-4.05 , 3.65]
D_2 1.501"	1 – 5	$k = 0.711x^2+0.994x+ 0.72$	[-2.70 , 3.30]
	2 – 6	$k = 1.08x^2-0.29x+ 1.213$	[-2.40 , 3.50]
	3 – 7	$k = 1.44x^2+0.538x+ 1.615$	[-2.45 , 3.00]
	4 – 8	$k = 1.254\ x^2+1.632x+ 2.23$	[-2.70 , 2.75]
D_3 1.499"	1 – 5	$k = 2.691x^2-2.212x+ 9.449$	[- 6.75, 5.20]
	2 – 6	$k = 3.465x^2-5.398x+ 9.771$	[-4.90 , 5.15]
	3 – 7	$k = 3.477x^2-2.908x+ 11.11$	[-4.85 , 4.25]
	4 – 8	$k = 3.192x^2-0.224x+ 10.85$	[-5.40 , 4.10]

Table 2. Maximum and minimum FB1 structural stiffness for the three shaft diameters

Journal Diameter	Angular Positions	Maximum K [lb/mil]	Minimum K [lb/mil]
D_1 1.500"	1 – 5	30.45 ± 0.52	2.75 ± 0.53
	2 – 6	32.65 ± 0.48	2.15 ± 0.42
	3 – 7	32.25 ± 0.60	2.99 ± 0.55
	4 – 8	33.84 ± 0.30	6.06 ± 0.55
D_2 1.501"	1 – 5	35.04 ± 0.66	9.45 ± 0.17
	2 – 6	42.69 ± 1.02	9.77 ± 0.33
	3 – 7	39.11 ± 1.62	11.12 ± 0.46
	4 – 8	34.79 ± 0.92	10.85 ± 0.04
D_3 1.499"	1 – 5	25.51 ± 0.58	0.72 ± 0.82
	2 – 6	29.10 ± 0.71	1.21 ± 0.16
	3 – 7	32.51 ± 0.52	1.62 ± 0.30
	4 – 8	29.99 ± 0.78	2.37 ± 1.02

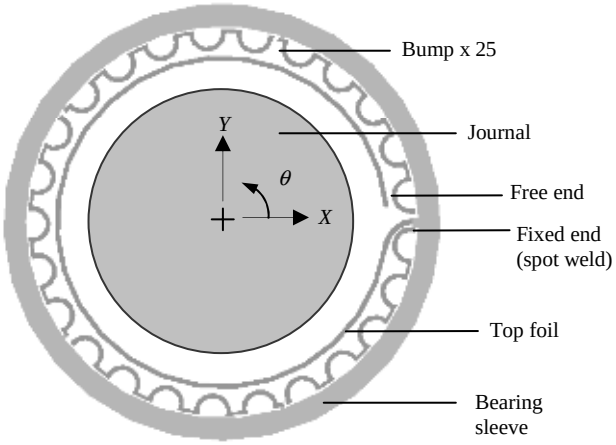

Figure 1. Schematic view bump type foil bearing features

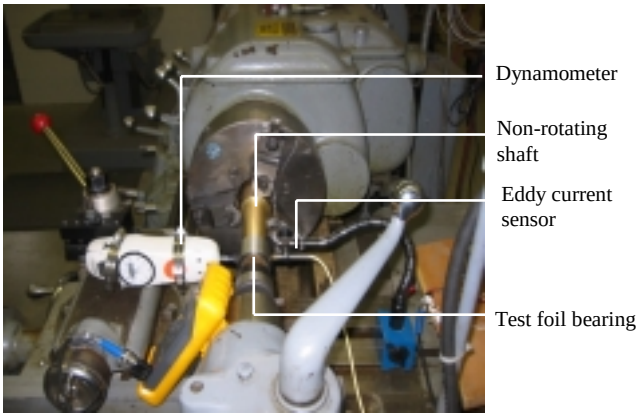

Figure 2. Test setup for static experiments

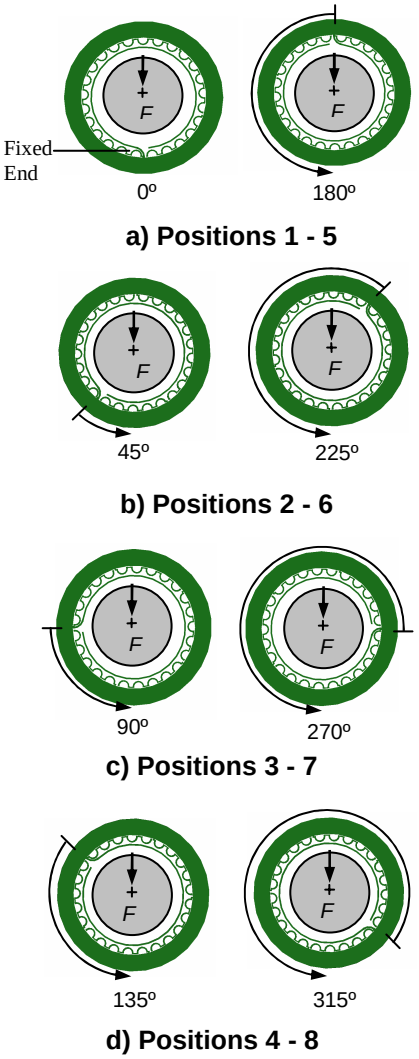

Figure 3. Labeled Angular Positions Grouped in Pairs

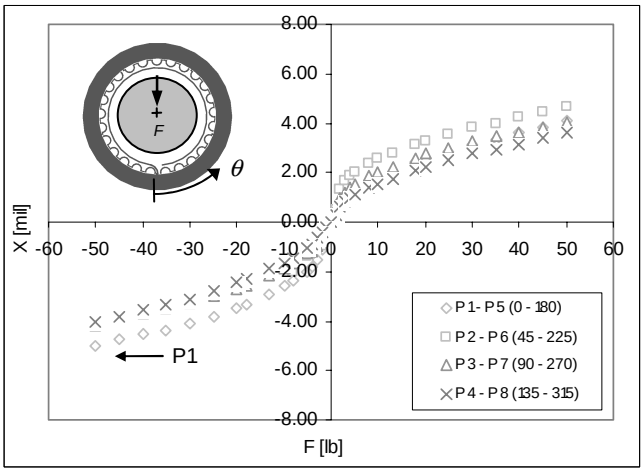

Figure 4. FB1 deflection versus static soad for all angular positions (journal diameter D_1 = 1.500")

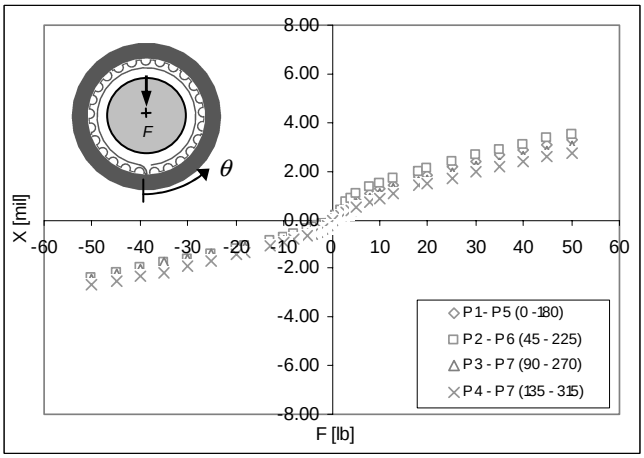

Figure 5. FB1 deflection versus static load for all angular positions (journal diameter D_2 = 1.501")

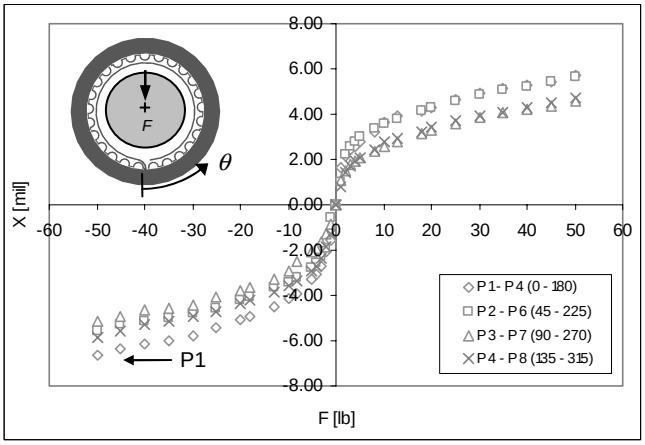

Figure 6. FB2 deflection versus static load for all angular positions (journal diameter D_3 = 1.499")

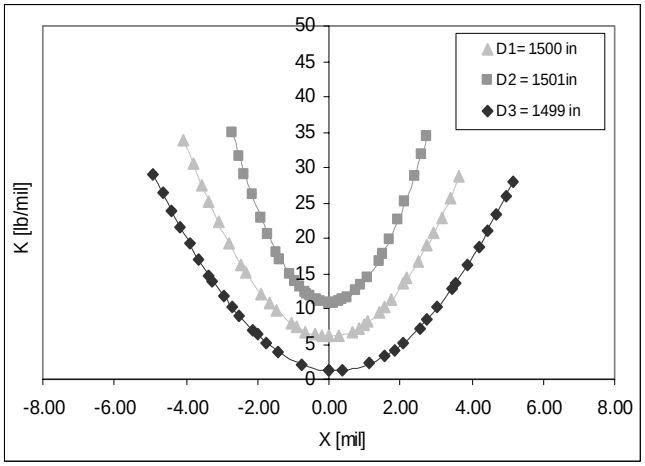

Figure 7. FB1 structural stiffness versus deflection for three different journal diameters. P4- P8 (135º-315º)

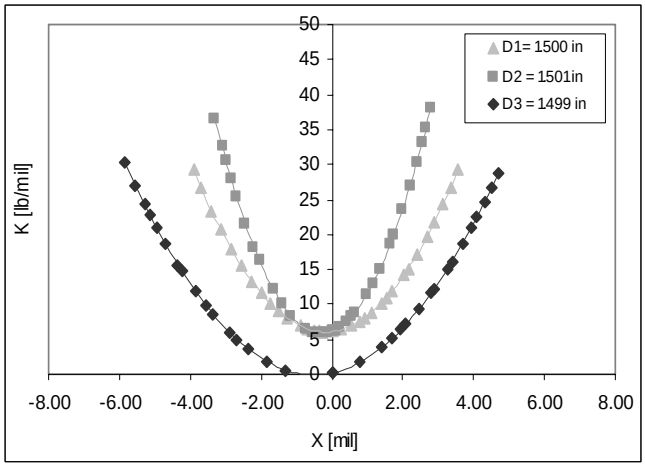

Figure 8. FB1 structural stiffness versus deflection for three different journal diameters. P4- P8 (135º-315º)

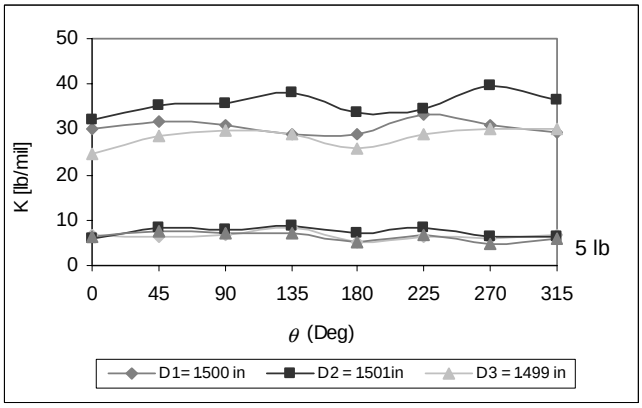

Figure 9.b FB2

Figure 9. Identified structural stiffness for all angular positions. Two static loads, 50 lb and 5 lb

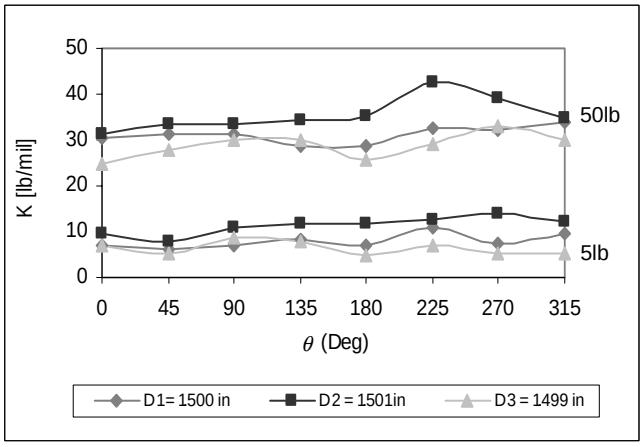

Figure 9.a. FB1

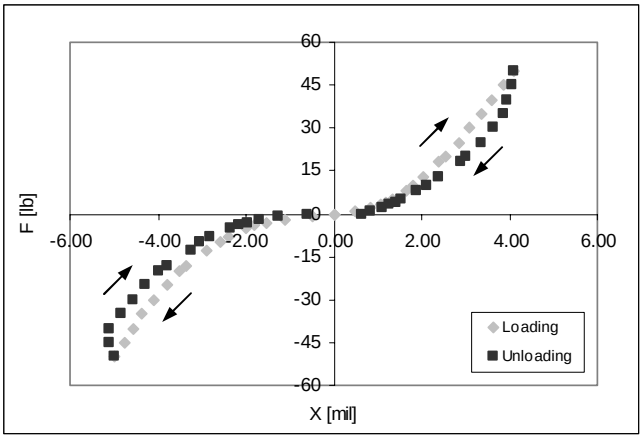

Figure 10. Hystesis FB1 for positions 1 - 5 (0º-180º) and using a D_1 journal nominal diameter

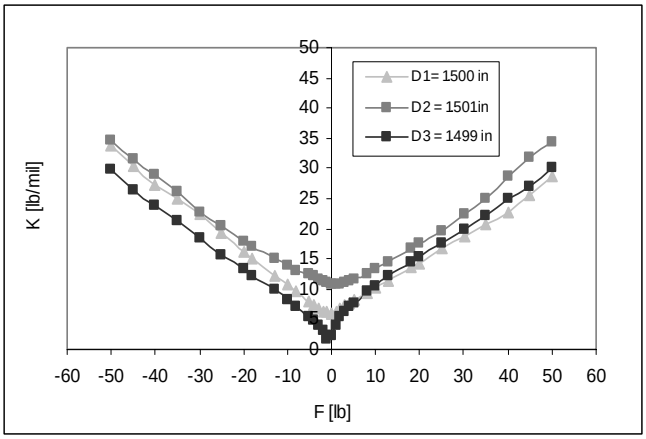

Figure 11. FB1 structural stiffness versus static load for three shaft diameters. Positions 4 – 8 (135°-315°)